the bodies appears to be tumor suppression (Hao et al. 1993; Juan et al. 2000). This finding, together with the identification of maternal uniparental disomy for chromosome 7 [upd(7)mat] in 7–10% of SRS patients (Hitchins et al. 2001), implies that SRS primarily represents an epigenetic disorder.

Notably, five monozygotic twin pairs discordant for SRS have been reported (Nyhan and Sakati 1977; Samn et al. 1990; Bailey et al. 1995; Sagot et al. 1996; Gicquel et al. 2005). In addition, the *H19*-DMR analysis has been performed in a single female twin pair, identifying a discordant methylation pattern (Gicquel et al. 2005). Here, we report monozygotic twins discordant for SRS and hypomethylation of the *H19*-DMR, and discuss underlying factors for such discordance.

Materials and methods

Case report

This Japanese female patient and her twin sister were conceived naturally to an unrelated and healthy 52-year-old father and 37-year-old mother. They were found to be monochorionic diamniotic twins by ultrasonographic studies at the first trimester. Because of the advanced maternal age, amniocentesis was carried out at 15 weeks of gestation, showing a 46,XX karyotype in both of the twins. The patient exhibited growth retardation since 20 weeks of gestation, while the twin sister grew well. Since the patient frequently showed decelerated fetal heart rate at 28 weeks of gestation, the twins were delivered by an emergent cesarean section.

At birth, the patient was 25.0 cm in length, 494 g in weight, and 24.0 cm in occipitofrontal head circumference (OFC), whereas the twin sister was 32.0 cm in length, 734 g in weight, and 24.5 cm in OFC (no reference growth data in neonates born at 28 weeks). Both twins were admitted to the neonatal intensive care unit and received respiratory and nutrition management for long terms (10 months for the patient and 5 months for the sister). The placenta of 280 g was shared by the twin, but there was no discernible interconnecting vascular anastomosis. At 2 years of age, the patient was diagnosed as having SRS on the basis of a constellation of clinical features that met the diagnostic criteria for SRS (Hitchins et al. 2001), such as pre- and postnatal growth failure, triangular face, relative macrocephaly, left hemihypotrophy, and bilateral fifth finger clinodactyly. Her psychomotor development appeared to be age-appropriate. Endocrine studies for short stature were normal, as were radiological studies. By contrast, the twin sister showed catch-up growth and manifested no SRS-like features. At 5 8/12 years of age, the patient measured 91.2 cm (−4.5 SD), weighed 12.8 kg (−2.1 SD), and had an OFC of 48.3 cm (−1.4 SD), whereas the twin sister measured 102.0 cm (−1.9 SD), weighed 13.6 kg (−1.9 SD), and had an OFC of 49.1 cm (−0.9 SD).

Microsatellite analysis

This study was approved by the Institutional Review Board Committee at the National Center for Child health and Development, and written informed consent was obtained from the parents. A total of 26 loci on multiple chromosomes were genotyped, using leukocyte genomic DNA. In brief, a segment encompassing each locus was PCR-amplified with a fluorescently labeled forward primer and an unlabeled reverse primer, and was determined for the physical size on an ABI PRISM 310 autosequencer using GeneScan software (Applied Biosystems, Foster City, CA).

Methylation analysis

Combined bisulfite restriction analysis (COBRA) and bisulfite sequencing were performed for two regions within the *H19*-DMR, i.e., a 317-bp region distal to the CTCF binding sites (DMR-A) (Vu et al. 2000) and a 435-bp region encompassing the CTCF binding site 6 (DMR-B), using leukocyte genomic DNA (Fig. 1a). The DMR-A and DMR-B were PCR-amplified with primers that hybridize to both methylated and unmethylated alleles because of absent CpG dinucleotides within the primer sequences.

For COBRA, the PCR products were digested with methylated allele-specific restriction enzymes (*Bsa*BI and *Mwo*I for the DMR-A; *Afl*III and *Hpy*188I for the DMR-B) (Fig. 1a). Subsequently, the methylation index was obtained using peak heights of digested and undigested fragments on the 2100 Bioanalyzer (Agilent, Santa Clara, CA). To define the normal range for the methylation indices, 40 control subjects were similarly studied.

For bisulfite sequencing, the PCR products were subcloned with TOPO TA Cloning Kit (Invitrogen, Carlsbad, CA), and multiple clones were subjected to direct sequencing on the CEQ 8000 autosequencer (Beckman Coulter, Fullerton, CA). The SNPs within the DMR-A (*rs2251375*) and the DMR-B (*rs11564736*, *rs10732516*, *rs34610866*, *rs2071094*, *rs35678657*, and *rs2107425*) were also genotyped, to identify the parental origin of each clone.

X-inactivation analysis

X-inactivation pattern was examined by the previously reported methods (Muroya et al. 1999). In brief, leukocyte genomic DNA was PCR-amplified with a

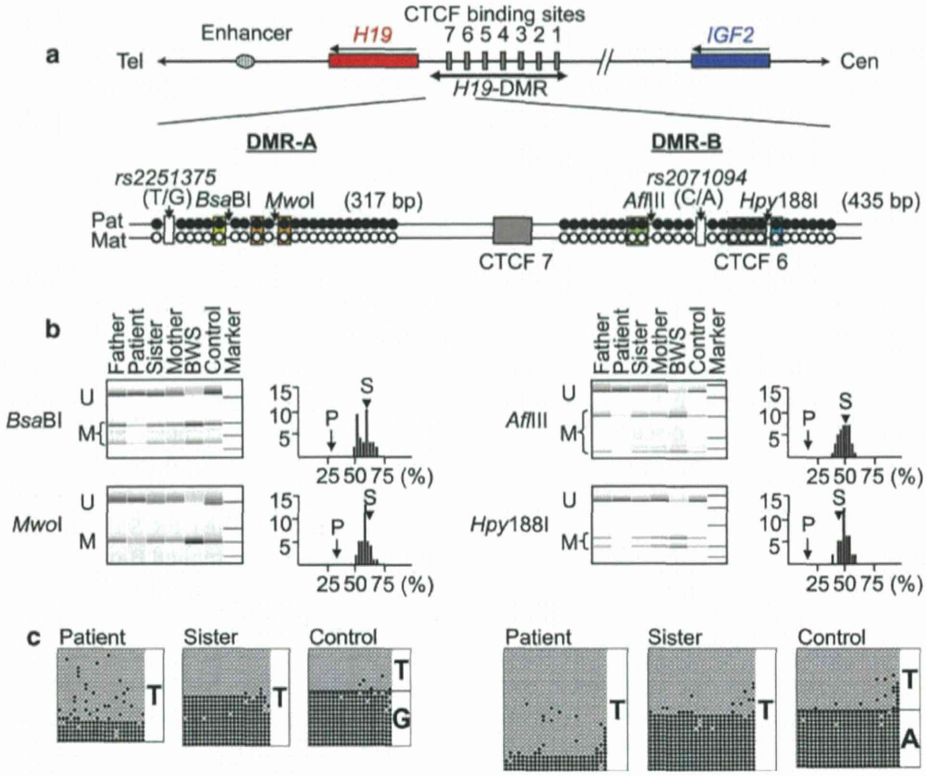

Fig. 1 Methylation analysis of the *H19*-DMR. **a** The regional physical map of the *IGF2-H19* imprinted domain and the location and the structure of the DMR-A and the DMR-B examined in this study. The *H19*-DMR resides in the upstream of *H19* and contains seven CTCF binding sites (shown in *gray boxes 1–7*). A common enhancer (shown with a *stippled ellipse*) is shared by the paternally expressed gene *IGF2* (shown in *blue*) and the maternally expressed gene *H19* (shown in *red*), and the enhancer exerts its effects on *IGF2* when the *H19*-DMR is methylated after paternal transmission (*filled circles*) and on *H19* when the *H19*-DMR is unmethylated after maternal transmission (*open circles*). The DMR-A (317 bp) resides distal to the CTCF binding sites and harbors 23 CpG dinucleotides, methylated allele-specific *Bsa*BI and *Mwo*I restriction sites, and the T/G SNP (*rs2251375*) (depicted with a *white box*). After bisulfite treatment, this region is digested with *Bsa*BI when the cytosine at the 6th CpG dinucleotide (indicated with a *yellow rectangle*) is methylated and with *Mwo*I when the two cytosines at the 9th and the 11th CpG dinucleotides (indicated with *two orange rectangles*) are methylated. The primer sequences used were: 5′-AACCCCTTCC-TACCACCATC-3′ and 5′-GGGTTTGGGAGAGTTTGTGA-3′. The DMR-B (435 bp) encompasses the CTCF binding site 6 (shown with a *gray box*) and contains 26 CpG dinucleotides, methylated allele-specific *Afl*III and *Hpy*188I restriction sites, and the C/A SNP (*rs2071094*) (depicted with a *white box*). After bisulfite treatment, this region is digested with *Afl*III when the cytosines at the eighth and the ninth CpG dinucleotides (indicated with *green rectangles*) are methylated and with *Hpy*188I when the cytosine at the 20th CpG dinucleotide (indicated with a *blue rectangle*) is methylated. The primer sequences used were: 5′-TGGGAGGAGATATTAGGGGA-ATA-3′ and 5′-TCCCAAACCATAACACTAAAACC-3′. **b** The results of the COBRA for the DMR-A (*left*) and the DMR-B (*right*). The actual electrophoresis images indicate that, for all the *Bsa*BI and the *Mwo*I sites in the DMR-A and the *Afl*III and the *Hpy*188I sites in the DMR-B, both unmethylated clone-specific bands (*U*) and methylated clone-specific bands (*M*) are found in the father, the sister, and the mother as well as in a control subject, whereas *U* is predominant in the patient and *M* is predominant in the Beckwith–Wiedemann syndrome (*BWS*) patient with upd(11p15)pat. As compared with the methylation indices of the normal control subjects depicted as histograms (the *horizontal axis* the methylation index with an interval of 2.5%; the *vertical axis* the subject number), the methylation indices of the patient (*P*) (shown with *arrows*) are below the normal range, and those of the twin sister (*S*) (shown with *arrowheads*) remain within the normal range. **c** Bisulfite sequencing results of the DMR-A (*left*) and the DMR-B (*right*) in the patient, the sister, and a control subject. *Each line* indicates a single clone, and each *circle* denotes a CpG dinucleotide; *filled* and *open circles* represent methylated and unmethylated cytosines, respectively. The T/G SNP (*rs2251375*) typing data within the DMR-A are indicated, as are the C/A SNP (*rs2071094*) typing data within the DMR-B (the *rs2071094* C allele has been converted into T allele after bisulfite treatment). The remaining five SNPs within the DMR-B were present in a homozygous status

fluorescently labeled forward primer and an unlabeled reverse primer flanking the highly polymorphic CAG repeat region and the two methylation sensitive *Hpa*II sites at exon 1 of *AR*, before and after *Hpa*II digestion (Fig. 2). The X-inactivation ratio was calculated using the area under curve after compensation for unequal amplification of the two alleles caused by the difference in the product size.

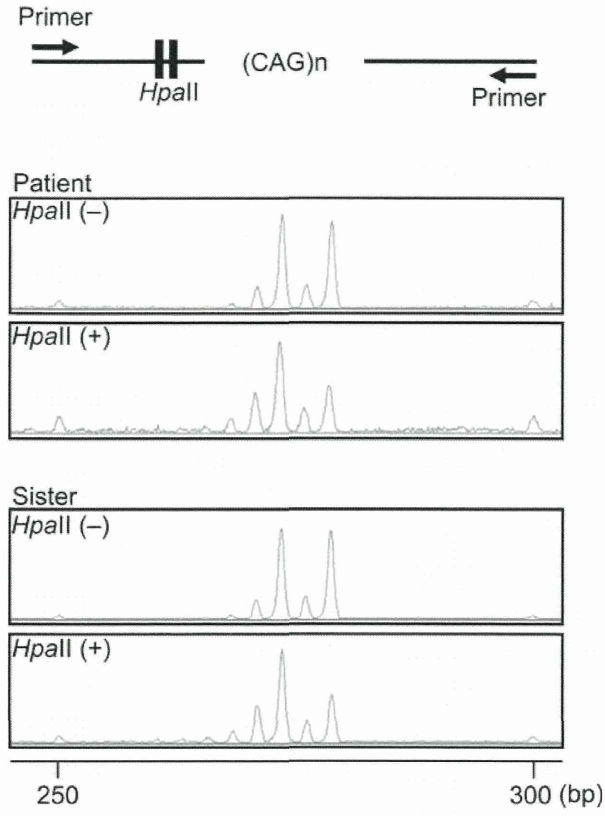

Fig. 2 X-inactivation analysis. The examined region contains a highly polymorphic CAG repeat region and two methylation sensitive *Hpa*II sites. Thus, PCR products are obtained from both active and inactive X chromosomes before *Hpa*II digestion and from inactive X chromosomes alone after *Hpa*II digestion. The comparison of the area under the *curves* between two heterozygous peaks (273 and 279 bp) before and after *Hpa*II digestion indicates that the two X chromosomes undergo random X-inactivation with nearly identical patterns between the twins. The small peaks are by-products caused by slippage phenomenon

Results

Microsatellite analysis

All the genotyping results were identical between the twins, indicating monozygosity (Table 1). Furthermore, upd(7)mat was excluded, as was upd(11p15)mat involving the *H19*-DMR.

Methylation analysis

The methylation indices of the patient (the DMR-A, 28.0% for the *Bsa*BI site and 30.4% for the *Mwo*I site; the DMR-B, 17.4% for the *Afl*III site and 17.1% for the *Hpy*188I site) were below the normal ranges (the DMR-A, 48.1–64.7% for the *Bsa*BI site and 50.1–67.6% for the *Mwo*I site; the DMR-B, 39.8–59.8% for the *Afl*III site and 39.3–58.0% for the *Hpy*188I site), whereas those of the twin sister, the father, and the mother were within the normal range (the DMR-A, 61.3, 61.7, and 62.3% for the *Bsa*BI site and 64.6, 64.9, and 61.0% for the *Mwo*I site; the DMR-B, 52.6, 52.7, and 51.5% for the *Afl*III site and 49.5, 50.4, and 52.9% for the *Hpy*188I site) (Fig. 1b). Furthermore, bisulfite sequencing revealed that the DMR-A and the DMR-B were predominantly hypomethylated in the patient and differentially methylated in the sister, although the SNP typing data for the seven SNPs were not informative for the parental origin of each clone in the twins (Fig. 1c). In the control subject, heterozygosity was detected for the T/G SNP (*rs2251375*) within the DMR-A and the C/A SNP (*rs2071094*) within the DMR-B, while the remaining five SNPs in the DMR-B were present in a homozygous status.

X-inactivation analysis

Both the patient and the twin sister had random X-inactivation with a nearly identical pattern (64%:36% for the patient and 65%:35% for the sister) (Fig. 2).

Discussion

We observed monozygotic twins discordant for SRS and identified hypomethylation of the *H19*-DMR (epimutation) in the affected twin only. In this regard, the clinical diagnosis of SRS in the affected twin was based on the criteria proposed by Hitchins et al. (2001), and the epimutation was clearly demonstrated for the two regions within the *H19*-DMR (DMR-A and DMR-B). Thus, although the difference in the clinical course might have some influence on the clinical and molecular discordance between the twins, the results imply that SRS in the affected twin is primarily caused by the epimutation occurring in the early fetal life.

The discordant methylation pattern of the *H19*-DMR may primarily be due to a failure to maintain the DNA methyltransferase-1 (DNMT1)-dependent methylation imprint around the pre-implantation S phase (Hirasawa et al. 2008). This notion has basically been suggested for monozygotic twins discordant for Beckwith–Wiedemann syndrome (BWS; MIM 130650) and hypomethylation of the KvDMR1 (Gaston et al. 2001; Weksberg et al. 2002). Indeed, such a failure would result in a hemimethylated daughter duplex that would subsequently be converted to a fully methylated and a fully unmethylated sister chromatid in the next S phase (Weksberg et al. 2002). This event would yield two different cell clones, one with normally methylated DMR with normal growth potential and the other with demethylated DMR with decreased growth potential, thereby leading to the separation of cells with different characters and resultant twinning discordant for

Table 1 The results of microsatellite analysis

Locus	Position	Mother	Patient	Sister	Father	Assessment
D3S1314	3q28	139	139/145	139/145	141/145	Biparental
D7S2846	7p14	177	177/181	177/181	181	Biparental
D7S519	7p13	261/263	261/263	261/263	261/263	NI
D7S1830	7p12	200	200/212	200/212	212	Biparental
D7S1870	7q11	118	118	118	118/120	NI
D7S634	7q21	136/144	138/144	138/144	126/138	Biparental
D7S527	7q21	291	291/295	291/295	273/295	Biparental
D7S1824	7q34	169/173	173	173	173	NI
D7S550	7q36	189/193	189	189	187/189	NI
D9S168	9p23	228/230	228/234	228/234	234/238	Biparental
D9S171	9p21	160/164	164/166	164/166	156/166	Biparental
D10S1580	10p12	140/148	140/150	140/150	142/150	Biparental
D10S198	10q24	183/197	183/197	183/197	183	NI
D10S1268	10q24	137/163	137	137	137	NI
D10S221	10q26	92/104	102/104	102/104	102	Biparental
D10S209	10q26	179	179/203	179/203	203	Biparental
D10S1700	10q26	125/127	125/127	125/127	123/127	NI
D11S2071	11p15	184/186	186/188	186/188	182/188	Biparental
D11S922	11p15	87/111	87	87	87	NI
D11S988	11p15	113	113/119	113/119	119/125	Biparental
D11S902	11p15	138/144	138/146	138/146	146/154	Biparental
D11S904	11p14	186/198	190/198	190/198	184/190	Biparental
D14S979	14q32	197/199	199/201	199/201	193/201	Biparental
D14S985	14q32	227/229	227/233	227/233	233/237	Biparental
D21S1446	21q22	206/222	206	206	206	NI
DXYS233	Xp22, Yp11	274/280	274/278	274/278	274/278	NI

NI not informative

The Arabic numbers indicate the PCR product sizes (bp). The primer sequences are available in the GDB Human Genome Database (http://www.gdb.org/)

SRS. Indeed, the methylation pattern of this patient would primarily be consistent with demethylation of the paternally derived *H19*-DMR in roughly half of cells. Although it might be possible that the *H19*-DMR hypomethylation took place after the twinning, this notion assumes no causal relationship between the *H19*-DMR hypomethylation and the twinning.

It may be worth pointing out that the twins were females. In this context, the sex ratio of previously reported five monozygotic twin pairs discordant for SRS is not remarkable with a male to female ratio of 2:3, and discordance for hypomethylation of the *H19*-DMR has been confirmed only in a single female twin pair (Nyhan and Sakati 1977; Samn et al. 1990; Bailey et al. 1995; Sagot et al. 1996; Gicquel et al. 2005). However, discordance for BWS and hypomethylation of the KvDMR1 is predominantly manifested by monozygotic female twins with a male to female ratio of 1:11 (Gaston et al. 2001; Weksberg et al. 2002). Since DNMT1 is also required for the maintenance of X-inactivation (Bestor 2000), this may have reduced the amount of DNMT1 enzyme available for the imprint maintenance of the DMRs, increasing the risk of demethylation of DMRs in the monozygotic female twins.

Hypomethylation of the *H19*-DMR was identified in leukocytes of this patient, but not in the twin sister. This contrasts the previous finding that *H19*-DMR in leukocytes is hypomethylated in both of the 11-year-old twin sisters discordant for SRS, whereas *H19*-DMR in skin fibroblasts is hypomethylated in the affected twin only (Gicquel et al. 2005). Such inconsistency may be due to the difference in placental vascular anatomy. While the present twins had no discernible interconnecting vascular anastomosis in the placenta, the twins described by Gicquel et al. (2005) may have shared fetal circulation, which allowed the transfer and engraftment of blood stem cells with demethylated *H19*-DMR from the affected twin to the unaffected twin. In this regard, since clinical features are similar between the

twins of this study and those reported by Gicquel et al. (2005), this implies that epimutations of the non-hematopoietic tissues such as skin fibroblasts are responsible for the development of SRS phenotype, whereas epimutations in leukocytes have no discernible clinical effects. For the present twins, since the X-inactivation pattern in leukocytes was nearly identical between the present twins in the probable absence of the shared fetal circulation, it may be that the X-inactivation pattern was established as a normal event simultaneously with, or just prior to, the demethylation of the *H19*-DMR as an abnormal event.

In summary, we identified monozygotic female twins discordant for SRS and the *H19*-DMR hypomethylation. This is reminiscent of hypomethylation of the KvDMR1 in one of the twin with BWS (Gaston et al. 2001; Weksberg et al. 2002). Since the *H19*-DMR and the KvDMR1 contiguously resides on chromosome 11p15, there may be a regional property for the occurrence of hypomethylation. Further studies will permit a better clarification of the prevalence of the monozygotic twins discordant for SRS and the mechanisms involved in this condition.

Acknowledgments This work was supported by Grants for Child Health and Development (20C-2) and for Research on Children and Families (H18-005) from the Ministry of Health, Labor, and Welfare, by Grants-in-Aid for Scientific Research (priority areas: 16086215; category B: 19390290) and for Young Scientists (B) (19790752) from the Ministry of Education, Culture, Sports, Science and Technology, and by a Grant from Kawano Masanori Memorial Foundation for Promotion of Pediatrics.

References

Bailey W, Popovich B, Jones KL (1995) Monozygotic twins discordant for the Russell–Silver syndrome. Am J Med Genet 58:101–105

Bell AC, Felsenfeld G (2000) Methylation of a CTCF-dependent boundary controls imprinted expression of the Igf2 gene. Nature 405:482–485

Bestor TH (2000) The DNA methyltransferases of mammals. Hum Mol Genet 9:2395–2402

Bliek J, Terhal P, van den Bogaard MJ, Maas S, Hamel B, Salieb-Beugelaar G, Simon M, Letteboer T, van der Smagt J, Kroes H, Mannens M (2006) Hypomethylation of the H19 gene causes not only Silver–Russell syndrome (SRS) but also isolated asymmetry or an SRS-like phenotype. Am J Hum Genet 78:604–614

Eggermann T, Schonherr N, Meyer E, Obermann C, Mavany M, Eggermann K, Ranke MB, Wollmann HA (2006) Epigenetic mutations in 11p15 in Silver–Russell syndrome are restricted to the telomeric imprinting domain. J Med Genet 43:615–616

Gaston V, Le Bouc Y, Soupre V, Burglen L, Donadieu J, Oro H, Audry G, Vazquez MP, Gicquel C (2001) Analysis of the methylation status of the KCNQ1OT and H19 genes in leukocyte DNA for the diagnosis and prognosis of Beckwith–Wiedemann syndrome. Eur J Hum Genet 9:409–418

Gicquel C, Rossignol S, Cabrol S, Houang M, Steunou V, Barbu V, Danton F, Thibaud N, Le Merrer M, Burglen L, Bertrand AM, Netchine I, Le Bouc Y (2005) Epimutation of the telomeric imprinting center region on chromosome 11p15 in Silver–Russell syndrome. Nat Genet 37:1003–1007

Hao Y, Crenshaw T, Moulton T, Newcomb E, Tycko B (1993) Tumour-suppressor activity of H19 RNA. Nature 365:764–767

Hark AT, Schoenherr CJ, Katz DJ, Ingram RS, Levorse JM, Tilghman SM (2000) CTCF mediates methylation-sensitive enhancer-blocking activity at the H19/Igf2 locus. Nature 405:486–489

Hirasawa R, Chiba H, Kaneda M, Tajima S, Li E, Jaenisch R, Sasaki H (2008) Maternal and zygotic Dnmt1 are necessary and sufficient for the maintenance of DNA methylation imprints during preimplantation development. Genes Dev 22:1607–1616

Hitchins MP, Stanier P, Preece MA, Moore GE (2001) Silver–Russell syndrome: a dissection of the genetic aetiology and candidate chromosomal regions. J Med Genet 38:810–819

Juan V, Crain C, Wilson C (2000) Evidence for evolutionarily conserved secondary structure in the H19 tumor suppressor RNA. Nucleic Acids Res 28:1221–1227

Leighton PA, Ingram RS, Eggenschwiler J, Efstratiadis A, Tilghman SM (1995a) Disruption of imprinting caused by deletion of the H19 gene region in mice. Nature 375:34–39

Leighton PA, Saam JR, Ingram RS, Stewart CL, Tilghman SM (1995b) An enhancer deletion affects both H19 and Igf2 expression. Genes Dev 9:2079–2089

Muroya K, Kosho T, Ogata T, Matsuo M (1999) Female carriers of Xp22.3 deletion including MRX locus. Am J Med Genet 84:384–385

Netchine I, Rossignol S, Dufourg MN, Azzi S, Rousseau A, Perin L, Houang M, Steunou V, Esteva B, Thibaud N, Demay MC, Danton F, Petriczko E, Bertrand AM, Heinrichs C, Carel JC, Loeuille GA, Pinto G, Jacquemont ML, Gicquel C, Cabrol S, Le Bouc Y (2007) 11p15 imprinting center region 1 loss of methylation is a common and specific cause of typical Russell–Silver syndrome: clinical scoring system and epigenetic-phenotypic correlations. J Clin Endocrinol Metab 92:3148–3154

Nyhan WL, Sakati NO (1977) Silver syndrome. In: Genetic and malformation syndromes in clinical medicine. Yearbook Medical Publisher, Chicago, pp 298–300

Sagot P, David A, Talmant C, Pascal O, Winer N, Boog G (1996) Russell–Silver syndrome: an explanation for discordant growth in monozygotic twins. Fetal Diagn Ther 11:72–78

Samn M, Lewis K, Blumberg B (1990) Monozygotic twins discordant for the Russell–Silver syndrome. Am J Med Genet 37:543–545

Thorvaldsen JL, Duran KL, Bartolomei MS (1998) Deletion of the H19 differentially methylated domain results in loss of imprinted expression of H19 and Igf2. Genes Dev 12:3693–3702

Vu TH, Li T, Nguyen D, Nguyen BT, Yao XM, Hu JF, Hoffman AR (2000) Symmetric and asymmetric DNA methylation in the human IGF2–H19 imprinted region. Genomics 64:132–143

Weksberg R, Shuman C, Caluseriu O, Smith AC, Fei YL, Nishikawa J, Stockley TL, Best L, Chitayat D, Olney A, Ives E, Schneider A, Bestor TH, Li M, Sadowski P, Squire J (2002) Discordant KCNQ1OT1 imprinting in sets of monozygotic twins discordant for Beckwith–Wiedemann syndrome. Hum Mol Genet 11:1317–1325

CLINICAL REPORT

AMERICAN JOURNAL OF medical genetics PART A

Somatic *CTNNB1* Mutation in Hepatoblastoma from a Patient with Simpson–Golabi–Behmel Syndrome and Germline *GPC3* Mutation

Rika Kosaki,[1] Toshiki Takenouchi,[2] Noriko Takeda,[3,4] Masayo Kagami,[5] Kazuhiko Nakabayashi,[6] Kenichiro Hata,[6] and Kenjiro Kosaki[2,7]*

[1]Division of Medical Genetics, National Center for Child Health and Development, Tokyo, Japan

[2]Department of Pediatrics, Keio University School of Medicine, Tokyo, Japan

[3]Department of Surgery, National Center for Child Health and Development, Tokyo, Japan

[4]Department of Surgery, Kitasato University, Kanagawa, Japan

[5]Department of Molecular Endocrinology, National Research Institute of Child Health and Development, Tokyo, Japan

[6]Department of Maternal-Fetal Biology, National Research Institute of Child Health and Development, Tokyo, Japan

[7]Center for Medical Genetics, Keio University School of Medicine, Tokyo, Japan

Manuscript Received: 28 June 2013; Manuscript Accepted: 20 October 2013

Simpson–Golabi–Behmel syndrome is a rare overgrowth syndrome caused by the *GPC3* mutation at Xq26 and is clinically characterized by multiple congenital abnormalities, intellectual disability, pre/postnatal overgrowth, distinctive craniofacial features, macrocephaly, and organomegaly. Although this syndrome is known to be associated with a risk for embryonal tumors, similar to other overgrowth syndromes, the pathogenetic basis of this mode of tumorigenesis remains largely unknown. Here, we report a boy with Simpson-Golabi–Behmel syndrome who had a germline loss-of function mutation in *GPC3*. At 9 months of age, he developed hepatoblastoma. A comparison of exome analysis results for the germline genome and for the tumor genome revealed a somatic mutation, p.Ile35Ser, within the degradation targeting box of β-catenin. The same somatic mutation in *CTNNB1* has been repeatedly reported in hepatoblastoma and other cancers. This finding suggested that the *CTNNB1* mutation in the tumor tissue represents a driver mutation and that both the *GPC3* and the *CTNNB1* mutations contributed to tumorigenesis in a clearly defined sequential manner in the propositus. The current observation of a somatic *CTNNB1* mutation in a hepatoblastoma from a patient with a germline *GPC3* mutation supports the notion that the mutation in *GPC3* may influence one of the initial steps in tumorigenesis and the progression to hepatoblastoma.

Key words: hepatoblastoma; Simpson–Golabi–Behmel syndrome; CTNNB1; GPC3

How to Cite this Article:
Kosaki R, Takenouchi T, Takeda N, Kagami M, Nakabayashi K, Hata K, Kosaki K. 2014. Somatic *CTNNB1* mutation in hepatoblastoma from a patient with Simpson–Golabi–Behmel syndrome and germline GPC3 mutation.
Am J Med Genet Part A 9999:1–5.

INTRODUCTION

Simpson–Golabi–Behmel syndrome (SGBS, OMIM312870) represents an overgrowth syndrome associated with organomegaly and macroglossia accompanied by characteristic external features, such as supernumerary nipples, supernumerary ribs, hypospadias, and cryptorchidism, as well as internal malformations, such as cardiac defects, diaphragmatic hernias, and cystic dysplasia of the kidneys [Cottereau et al., 2013]. SGBS is caused by loss-of-function mutations in the heparan sulphate proteoglycan, glypican 3 gene (*GPC3*) at chromosome Xq26 [Pilia et al., 1996]. The *GPC3* gene encodes an extracellular matrix protein that is expressed during development and that regulates cell proliferation and apoptosis during

Conflict of interest: none.
Grant sponsor: Ministry of Health, Labour and Welfare, Japan the Health and Labour Sciences Research Grant for Research on rare and intractable diseases (Jitsuyoka(Nanbyo)-Ippan-003 & 13).
*Correspondence to:
Kenjiro Kosaki, M.D., Center for Medical Genetics, Keio University School of Medicine 35 Shinanomachi, Shinjuku-ku, Tokyo 160-8582, Japan. E-mail: kkosaki@z3.keio.jp
Article first published online in Wiley Online Library (wileyonlinelibrary.com): 00 Month 2013
DOI 10.1002/ajmg.a.36364

development through the modulation of growth factor action, including that of IGF2 [Gonzalez et al., 1998; Pellegrini et al., 1998].

Patients with SGBS are at an increased risk for the development of embryonal tumors, such as Wilms tumor [Xuan et al., 1994; Hughes-Benzie et al., 1996; Lindsay et al., 1997] and hepatoblastoma [Lapunzina et al., 1998; Li et al., 2001; Buonuomo et al., 2005; Mateos et al., 2013]. In a recent article published in this journal, Mateos et al. [2013] documented a patient with SGBS and a *GPC3* duplication who developed a hepatoblastoma. The pathogenetic basis of the triggering and progression of embryonal tumors in the absence of a functional *GPC3* is currently unknown. Here, we document an infant with a *GPC3* mutation who developed a hepatoblastoma in which the tissue was shown to harbour a *CTNNB1* mutation using exome sequencing. This observation sheds new insight on the stepwise progression of hepatoblastoma.

CLINICAL REPORT

The propositus was born at 41 weeks of gestation as the first child of nonconsanguineous parents. He was delivered by cesarean section. His mother was 35 years old, had a height of 165 cm (+1.3 SD), and had coarse facial features. The father was 54 years old and was healthy. The birth weight of the propositus was 4,068 g (+2.65 SD), his length was 55 cm (+2.8 SD), and his head circumference was 37.5 cm (+2.66 SD). He had a ventricular septal defect that was repaired at the age of 1 month.

At the age of 4 months, his weight was 8.55 kg (+1.61 SD), his length was 68.8 cm (+1.71 SD), and his head circumference was 43.8 cm (+1.6 SD). He had an upturned bulbous nose, a wide nasal bridge, apparent hypertelorism, macrostomia, macroglossia, a midline grooved tongue, a right accessory nipple, and a short webbed neck. His hands were broad, and he had right index fingernail hypoplasia. Based on these clinical features, he was diagnosed as having SGBS (Fig. 1A). Regular surveillance was started to screen for the possible development of abdominal tumors, including hepatoblastoma and Wilms tumor. A cystic lesion was detected in the hepatic parenchyma at 9 months during an abdominal ultrasound examination. An abdominal CT scan revealed a 45 mm × 35 mm × 35 mm heterogeneously enhancing mass localized in S4 that was classified as PRETEXT stage III (Fig 1B,C). The patient's serum α-fetoprotein was elevated to 658 ng/ml. A fine needle biopsy led to a pathological diagnosis of hepatoblastoma. After chemotherapy with cisplatin and tetrahydropyranyladriamycin, the residual mass was surgically removed at the age of 14 months. At the age of 2 years, he continued to demonstrate overgrowth, with a weight of 17.1 kg (+4.58 SD) and a length of 95.7 cm (+3.4 SD).

MOLECULAR INVESTIGATION

Informed consent from the parents and approval from the institutional review board were obtained for the molecular studies. We first performed Sanger sequencing of the *GPC3* gene using DNA obtained from a peripheral blood sample of the propositus. A c.1159C > T, p.Arg387X mutation was identified, confirming the diagnosis of SGBS. Next, we obtained DNA from the hepatoblastoma tissue resected at the time of biopsy. A matched non-tumor

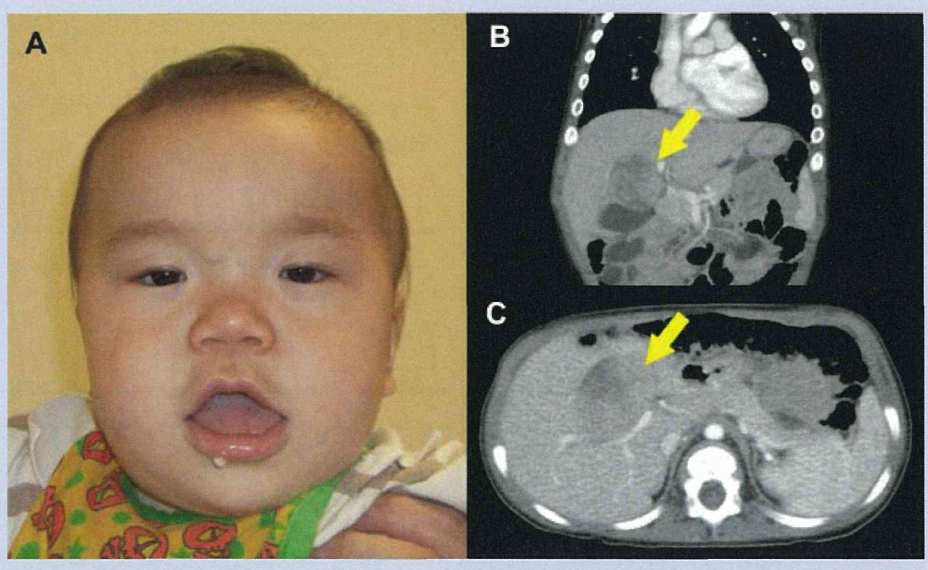

FIG. 1. The characteristic facial features and hepatoblastoma in the propositus. A: Note that the facial features of the propositus included upturned bulbous nose, a wide nasal bridge, apparent hypertelorism, macrostomia, macroglossia, and a midline grooved tongue. B and C: Coronal (B) and axial (C) slices of magnetic resonance imaging at 9 months of age showed a well-demarcated heterogeneously enhancing mass, measuring 45 mm × 35 mm × 35 mm, in S4 of the liver (yellow arrows).

peripheral blood DNA sample was also obtained. Whole-exome sequencing was performed for both DNA samples. Massive parallel sequencing on an Illumina HiSEQ platform yielded ~11 gigabases per sample, with a mean coverage of 114-fold across 54 Mb of targeted coding regions (SureSelectXT2 Human All Exon V4; Agilent Technologies, Santa Clara, CA) for each sample. The sequence reads were aligned to the reference genome assemblies (hg19) using BWA [Li and Durbin, 2009]. Local realignment around the insertions/deletions and base quality score recalibration were performed using the Genome Analysis Tool Kit software [McKenna et al., 2010], with duplicate reads removed using Picard. On average, 73% of the coding bases were covered in sufficient depth in both the tumor and the matched normal samples to allow for confident mutation detection.

MuTect version 1.14 [Cibulskis et al., 2013] was used for comparison of the exome data derived from hepatoblastoma and that derived from the peripheral blood. The default parameters were used except that max_alt_alleles_in_normal_count and minimum_mutation_cell_fraction were set to 0 and 0.1, respectively. The Mutect program detected seventy mutations as a somatic change. These 70 mutations were annotated by the program SnpEff [Cingolani et al., 2012] and classified into the following classes of mutations: non-synonymous coding, non-synonymous start, splice site acceptor, splice site donor, start lost, stop gained, and stop lost. A mutation c.104T > G, p.Ile35Ser (NM_00904) was identified at exon 3 of the *CTNNB1* that encodes β-catenin, and was the only remaining somatic mutation through the filtering process described above. This alteration was confirmed using Sanger sequencing (Fig. 2). An analysis of the reads at the mutant position after the removal of duplicated reads revealed that 72 out of 171 reads were mutant.

Mutations within a targeting box are known to lead to the accumulation of intracytoplasmic and nuclear β-catenin protein [Koch et al., 1999; Purcell et al., 2011]. The catalog of somatic mutations in cancer (COSMIC) version 64 database contained 28 instances of samples containing the somatic mutation p.Ile35Ser in *CTNNB1* under the query conditions "confirmed somatic" or "previously reported"; "tumor sample, not cultured"; and "not reported as polymorphism in the 1,000 genome projects". Out of the 29 samples, 21 originated from the liver, 2 from soft tissue, and 1 each from the endometrium, pituitary, thymus, central nervous system, and lung. Hence, most of, if not all, the samples with p.Ile35Ser were derived from the liver. Among the 21 samples, 4 samples were specifically labeled as hepatoblastoma samples; in the remaining samples, the patient's age was not mentioned, and the clinical distinction between hepatocellular carcinoma versus hepatoblastoma was not mentioned. Furthermore, a literature review on *CTNNB1* mutation analyses in hepatoblastomas in patients without multiple malformation syndromes indicated that at least five patients carried the c.104T > G, p.Ile35Ser mutation [Takayasu et al., 2001; Cairo et al., 2008; Lopez-Terrada et al., 2009; Purcell et al., 2011; Chavan et al., 2012]. The article by Takayasu et al. was not catalogued in the COSMIC database.

DISCUSSION

Through Bayesian comparison of the exome data between the germline genome and the tumor genome, we identified a somatic *CTNNB1* mutation, p.Ile35Ser, within the degradation targeting box of β-catenin in the hepatoblastoma tissue of a patient with an overgrowth syndrome, SGBS, who had a loss-of-function mutation in the *GPC3* gene.

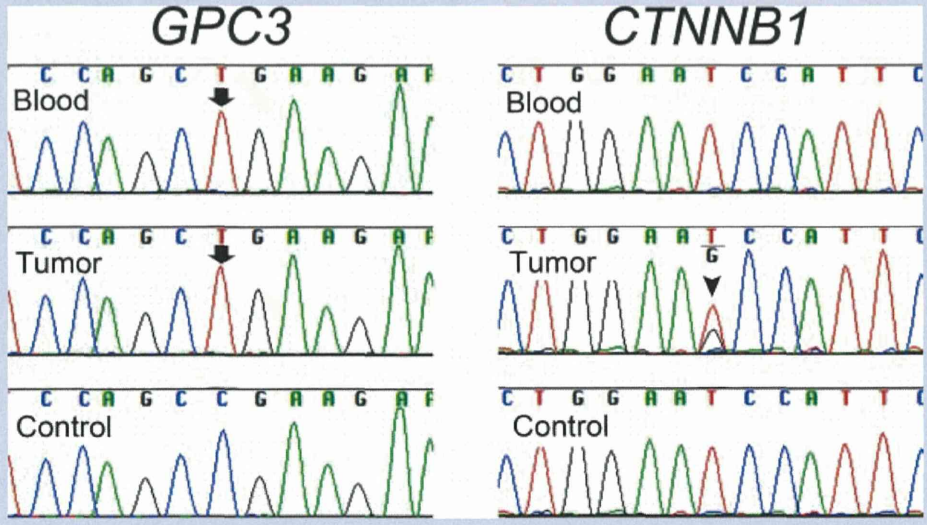

FIG. 2. Partial DNA sequences, including the sequences containing the mutations in the *GPC3* and *CTNNB1* genes. In a blood sample, a hemizygous mutation, c.1159C > T (top arrow), was identified in *GPC3*, but no mutations were identified in *CTNNB1*. In tumor tissue, a hemizygous mutation, c.1159C > T (bottom arrow), was identified in *GPC3* and a heterozygous mutation, c.104T > G (arrowhead), was identified in *CTNNB1*. The control shows a normal peripheral blood sample from a normal individual.

In general, the mutations identified in tumor tissue can be classified into two groups [Burgess, 2013]: "Driver mutations" that are directly involved in tumorigenesis followed by tumor progression, and "passenger mutations" that are not responsible for tumorigenesis or tumor progression but are by-products of genomic instability in tumor cells and are biologically neutral. A distinguishing feature of driver mutations is the recurrent appearance of the same somatic mutation in different individuals. Since the p.Ile35Ser mutation has been reported at least five times in hepatoblastomas [Takayasu et al., 2001; Cairo et al., 2008; Lopez-Terrada et al., 2009; Purcell et al., 2011; Chavan et al., 2012] and 17 times in samples from non-hepatoblastoma liver tumors, including hepatocellular carcinoma, it is reasonable to assume that the p.Ile35Ser *CTNNB1* mutation in the tumor tissue from the propositus represents a driver mutation.

The software MuTect has been shown to be efficient at detecting somatic mutations in a relatively small percentage (i.e., <10%) of tumor cells in a normal tissue background. Hence, the chance of missing mutations in other genes that are present in a subset of the cells in the tumor tissue is unlikely to be very high. Nevertheless, the classes of mutations that have been missed could include but are not limited to: (1) mutations in low coverage areas; (2) mutations in non-coding portions of the genome, such as in non-coding RNAs or regulatory elements; and (3) epigenetic changes that are undetectable using exome sequencing.

The identification of the *CTNNB1* mutation in a patient with SGBS sheds new light on the pathogenesis of hepatoblastoma: *CTNNB1* mutations within a targeting box, in which the propositus' p.Ile35Ser mutation resided, are known to lead to the accumulation of intracytoplasmic and nuclear β-catenin protein and to potentiate canonical Wnt/β-catenin signaling [Koch et al., 1999; Purcell et al., 2011]. Of note, the loss of Gpc3 leads to the activation of canonical Wnt/β-catenin signaling in *Gpc3*-knockout mice [Song et al., 2005]. If this finding is extrapolated to humans, the *GPC3* loss-of-function mutation could have exerted an additive effect on the potentiation of canonical Wnt/β-catenin signaling by the *CTNNB1* mutation. Given the fact that the propositus harbored a germline *GPC3* mutation and that the tumor harbored a somatic *CTNNB1* mutation together with the *GPC3* mutation, *GPC3* and *CTNNB1* apparently contributed to tumorigenesis in a clearly defined sequential manner, at least in the propositus. Whether mutations in *GPC3* and *CTNNB1* must occur in this specific sequence, and not vice versa, remains uncertain. Somatic loss-of-function mutations in *GPC3* have been reported in tumor tissues with various origins, including the lung (6/18), kidney (3/18), endometrium (3/18), large intestine (2/18), breast (1/18), prostate (1/18), and skin (2/18), but not in the liver according to the COSMIC database, version 66 [Forbes et al., 2011], and a search performed under the query conditions "confirmed somatic" or "previously reported"; "tumor sample, not cultured"; and "not reported" as polymorphism in the 1,000 genome projects. Hence, mutations in *GPC3* are unlikely to yield a liver-tumor-specific susceptibility to tumorigenesis or tumor progression.

From an etiological standpoint, SGBS and another prototypic overgrowth syndrome, Beckwith–Wiedemann syndrome (BWS, OMIM130650), share a key fetal growth accelerator, IGF2: the overproduction of IGF2 in BWS and the lack of an anchoring action of IGF2 by the extracellular matrix protein GPC3 in SGBS both promote fetal growth. Patients with BWS are known to have an increased susceptibility to hepatoblastoma, similar to patients with SGBS [Fukuzawa et al., 2003]. Further elucidation of the role of the *CTNNB1* mutation in hepatoblastomas in patients with BWS is warranted. Similarly, the likely role of *CTNNB1* mutation in the pathogenesis of Wilms tumor in both SGBS and BWS should be explored, together with the potential role of *GPC3* mutation in isolated hepatoblastomas.

In summary, we here document a somatic *CTNNB1* mutation in a hepatoblastoma from a patient with SGBS and a germline *GPC3* mutation. The current observation supports the notion that a mutation in *GPC3* may represent an initial step in the tumorigenesis and progression of hepatoblastoma.

ACKNOWLEDGMENTS

This work was supported by the Health and Labour Sciences Research Grant for Research on rare and intractable diseases (Jitsuyoka(Nanbyo)-Ippan-003) and Research on Applying Health Technology (H23-013) from the Ministry of Health, Labour and Welfare, Japan. We thank Ms. Yumi Obayashi for her technical assistance in article preparation.

REFERENCES

Buonuomo PS, Ruggiero A, Vasta I, Attina G, Riccardi R, Zampino G. 2005. Second case of hepatoblastoma in a young patient with Simpson-Golabi-Behmel syndrome. Pediatr Hematol Oncol 22:623–628.

Burgess DJ. 2013. Tumour evolution: Weighed down by passengers? Nat Rev Cancer 13:219.

Cairo S, Armengol C, De Reynies A, Wei Y, Thomas E, Renard CA, Goga A, Balakrishnan A, Semeraro M, Gresh L, Pontoglio M, Strick-Marchand H, Levillayer F, Nouet Y, Rickman D, Gauthier F, Branchereau S, Brugieres L, Laithier V, Bouvier R, Boman F, Basso G, Michiels JF, Hofman P, Arbez-Gindre F, Jouan H, Rousselet-Chapeau MC, Berrebi D, Marcellin L, Plenat F, Zachar D, Joubert M, Selves J, Pasquier D, Bioulac-Sage P, Grotzer M, Childs M, Fabre M, Buendia MA. 2008. Hepatic stem-like phenotype and interplay of Wnt/beta-catenin and Myc signaling in aggressive childhood liver cancer. Cancer Cell 14:471–484.

Chavan RS, Patel KU, Roy A, Thompson PA, Chintagumpala M, Goss JA, Nuchtern JG, Finegold MJ, Parsons DW, Lopez-Terrada DH. 2012. Mutations of PTCH1, MLL2, and MLL3 are not frequent events in hepatoblastoma. Pediatr Blood Cancer 58:1006–1007.

Cibulskis K, Lawrence MS, Carter SL, Sivachenko A, Jaffe D, Sougnez C, Gabriel S, Meyerson M, Lander ES, Getz G., 2013. Sensitive detection of somatic point mutations in impure and heterogeneous cancer samples. Nat Biotechnol 31:213–219.

Cingolani P, Platts A, Wang le L, Coon M, Nguyen T, Wang L, Land SJ, Lu X, Ruden DM. 2012. A program for annotating and predicting the effects of single nucleotide polymorphisms, SnpEff: SNPs in the genome of Drosophila melanogaster strain w1118; iso-2; iso-3. Fly (Austin) 6:80–92.

Cottereau E, Mortemousque I, Moizard MP, Burglen L, Lacombe D, Gilbert-Dussardier B, Sigaudy S, Boute O, David A, Faivre-Olivier L, Amiel J, Robertson R, Viana Ramos F, Bieth E, Odent S, Demeer B, Mathieu M, Gaillard D, Van Maldergem L, Baujat G, Maystadt I, Heron D, Verloes A, Philip N, Cormier-Daire V, Froute MF, Pinson L, Blanchet P, Sarda P, Willems M, Jacquinet A, Ratbi I, van den Ende J, Lackmy-Port Lis M, Goldenberg A, Bonneau D, Rossignol S, Toutain A. 2013.

Phenotypic spectrum of simpson-golabi-behmel syndrome in a series of 42 cases with a mutation in GPC3 and review of the literature. Am J Med Genet C Semin Med Genet 163C:92–105.

Forbes SA, Bindal N, Bamford S, Cole C, Kok CY, Beare D, Jia M, Shepherd R, Leung K, Menzies A, Teague JW, Campbell PJ, Stratton MR, Futreal PA. 2011. COSMIC: Mining complete cancer genomes in the catalogue of somatic mutations in cancer. Nucleic Acids Res 39:D945–D950.

Fukuzawa R, Hata J, Hayashi Y, Ikeda H, Reeve AE. 2003. Beckwith-Wiedemann syndrome-associated hepatoblastoma: Wnt signal activation occurs later in tumorigenesis in patients with 11p15.5 uniparental disomy. Pediatr Dev Pathol 6:299–306.

Gonzalez AD, Kaya M, Shi W, Song H, Testa JR, Penn LZ, Filmus J. 1998. OCI-5/GPC3, a glypican encoded by a gene that is mutated in the Simpson-Golabi-Behmel overgrowth syndrome, induces apoptosis in a cell line-specific manner. J Cell Biol 141:1407–1414.

Hughes-Benzie RM, Pilia G, Xuan JY, Hunter AG, Chen E, Golabi M, Hurst JA, Kobori J, Marymee K, Pagon RA, Punnett HH, Schelley S, Tolmie JL, Wohlferd MM, Grossman T, Schlessinger D, MacKenzie AE. 1996. Simpson-Golabi-Behmel syndrome: Genotype/phenotype analysis of 18 affected males from 7 unrelated families. Am J Med Genet 66:227–234.

Koch A, Denkhaus D, Albrecht S, Leuschner I, von Schweinitz D, Pietsch T. 1999. Childhood hepatoblastomas frequently carry a mutated degradation targeting box of the beta-catenin gene. Cancer Res 59:269–273.

Lapunzina P, Badia I, Galoppo C, De Matteo E, Silberman P, Tello A, Grichener J, Hughes-Benzie R. 1998. A patient with Simpson-Golabi-Behmel syndrome and hepatocellular carcinoma. J Med Genet 35:153–156.

Li H, Durbin R. 2009. Fast and accurate short read alignment with Burrows-Wheeler transform. Bioinformatics 25:1754–1760.

Li M, Shuman C, Fei YL, Cutiongco E, Bender HA, Stevens C, Wilkins-Haug L, Day-Salvatore D, Yong SL, Geraghty MT, Squire J, Weksberg R. 2001. GPC3 mutation analysis in a spectrum of patients with overgrowth expands the phenotype of Simpson-Golabi-Behmel syndrome. Am J Med Genet 102:161–168.

Lindsay S, Ireland M, O'Brien O, Clayton-Smith J, Hurst JA, Mann J, Cole T, Sampson J, Slaney S, Schlessinger D, Burn J, Pilia G. 1997. Large scale deletions in the GPC3 gene may account for a minority of cases of Simpson-Golabi-Behmel syndrome. J Med Genet 34:480–483.

Lopez-Terrada D, Gunaratne PH, Adesina AM, Pulliam J, Hoang DM, Nguyen Y, Mistretta TA, Margolin J, Finegold MJ. 2009. Histologic subtypes of hepatoblastoma are characterized by differential canonical Wnt and Notch pathway activation in DLK+ precursors. Hum Pathol 40:783–794.

Mateos ME, Beyer K, Lopez-Laso E, Siles JL, Perez-Navero JL, Pena MJ, Guzman J, Matas J. 2013. Simpson-golabi-behmel syndrome type 1 and hepatoblastoma in a patient with a novel exon 2-4 duplication of the GPC3 gene. Am J Med Genet Part A 161A:1091–1095.

McKenna A, Hanna M, Banks E, Sivachenko A, Cibulskis K, Kernytsky A, Garimella K, Altshuler D, Gabriel S, Daly M, DePristo MA. 2010. The genome analysis toolkit: A Mapreduce framework for analyzing next-generation DNA sequencing data. Genome Res 20:1297–1303.

Pellegrini M, Pilia G, Pantano S, Lucchini F, Uda M, Fumi M, Cao A, Schlessinger D, Forabosco A. 1998. Gpc3 expression correlates with the phenotype of the Simpson-Golabi-Behmel syndrome. Dev Dyn 213:431–439.

Pilia G, Hughes-Benzie RM, MacKenzie A, Baybayan P, Chen EY, Huber R, Neri G, Cao A, Forabosco A, Schlessinger D. 1996. Mutations in GPC3, a glypican gene, cause the Simpson-Golabi-Behmel overgrowth syndrome. Nat Genet 12:241–247.

Purcell R, Childs M, Maibach R, Miles C, Turner C, Zimmermann A, Sullivan M. 2011. HGF/c-Met related activation of beta-catenin in hepatoblastoma. J Exp Clin Cancer Res 30:96.

Song HH, Shi W, Xiang YY, Filmus J. 2005. The loss of glypican-3 induces alterations in Wnt signaling. J Biol Chem 280:2116–2125.

Takayasu H, Horie H, Hiyama E, Matsunaga T, Hayashi Y, Watanabe Y, Suita S, Kaneko M, Sasaki F, Hashizume K, Ozaki T, Furuuchi K, Tada M, Ohnuma N, Nakagawara A. 2001. Frequent deletions and mutations of the beta-catenin gene are associated with overexpression of cyclin D1 and fibronectin and poorly differentiated histology in childhood hepatoblastoma. Clin Cancer Res 7:901–908.

Xuan JY, Besner A, Ireland M, Hughes-Benzie RM, MacKenzie AE. 1994. Mapping of Simpson-Golabi-Behmel syndrome to Xq25-q27. Hum Mol Genet 3:133–137.